One-Pot, Facile, and Versatile Synthesis of Monolayer MoS_2/WS_2 Quantum Dots as Bioimaging Probes and Efficient Electrocatalysts for Hydrogen Evolution Reaction

*Shengjie Xu, Dian Li, and Peiyi Wu**

In this work, uniform molybdenum disulfide (MoS_2)/tungsten disulfide (WS_2) quantum dots are synthesized by the combination of sonication and solvothermal treatment of bulk MoS_2/WS_2 at a mild temperature. The resulting products possess monolayer thickness with an average size about 3 nm. The highly exfoliated and defect-rich structure renders these quantum dots plentiful active sites for the catalysis of hydrogen evolution reaction (HER). The MoS_2 quantum dots exhibit a small HER overpotential of ≈120 mV and long-term durability. Moreover, the strong fluorescence, good cell permeability, and low cytotoxicity make them promising and biocompatible probes for in vitro imaging. In addition, this work may provide an alternative facile approach to synthesize the quantum dots of transition metal dichalcogenides or other layered materials on a large scale.

1. Introduction

Following the discovery of graphene, great attention has been paid to other layered materials due to the exotic electronic properties and high specific surface areas which are important for sensors, transistors, catalysis, photodetectors, lithium ion batteries, and energy storage applications.[1,2] Although graphene is the most well-known 2D single-layer material, layered transition metal dichalcogenides (LTMDs) form a large family of layered materials with interesting properties, whose crystal structures are built up of covalently bonded X–M–X (M = Mo, W; X = S, Se, Te) single layers which interact by Van der Waals forces like graphite and can be easily cleaved along the layer plane.[3–5] Among these, molybdenum disulfide (MoS_2), a widely known LTMD, is traditionally used as solid-state lubricants, catalysts for hydrodesulfurization, and hydrogen evolution as well as photovoltaic and photocatalytic materials.[6] Recent works have been reported that the band-gap of MoS_2 can be tuned from an indirect band-gap (1.2 eV for bulk form) to a direct band-gap (1.9 eV for monolayer) with the decrease in layer thickness.[3,4,7,8] Hence, this material has drawn great attention in many new fields, such as energy storage, gas sensing, solar cell, catalysis, and electronic devices, etc. Besides, Liu et al. have found MoS_2/tungsten disulfide (WS_2) nanosheets also can be utilized for the biomedicine, including bioimaging, therapy, and toxicity through a succession of postmodification for enhancing the compatibility in physiological environments.[9]

Since the hydrogen binding energy of MoS_2 is close to that of Pt-group metals, MoS_2 and their composites have been regarded as promising substitutes for traditional Pt-group metals which are expensive and scarce in hydrogen evolution reaction (HER).[10,11] However, the limitation of active edges, electrical conductivity, as well as special surface area of MoS_2 nanostructure have hindered the widespread use of MoS_2-based catalysts for efficient evolution of hydrogen. Thereby, an endeavor of intensive researches has focused on the achievement of more active sites at the edge and higher special surface area which are crucial to the catalytic activity toward HER. To date, many strategies have been proposed, such as fabrication of MoS_2 nanosheets, preparation of mesoporous MoS_2, synthesis of the composites of MoS_2 layers and metal nanoparticles or graphene, etc.[8,12,13] Among these, single or few-layer MoS_2 nanosheets have attracted great attention and been widely utilized, due to the facile preparation process along with more active sites, higher carrier mobility, and special surface area of as-prepared catalysts.[14,15]

Traditionally, single or few-layer MoS_2/WS_2 nanosheets can be obtained by many methods, including chemical vapor deposition, thermal ablation method, mechanical and chemical exfoliation, and direct solvothermal synthesis. Among these available methods, chemical exfoliation is the most suitable route for the large scale production of nanosheets, due to other methods always suffer from more or less drawbacks, such as requirement for expensive systems, low efficiency, long and complex process, and severe synthetic conditions, which distinctly hinder the widespread use of them.[2,8,16–18] Conventionally, MoS_2/WS_2 nanosheets can be massively prepared by exfoliating bulk crystals of MoS_2/WS_2 with Li-intercalation followed by reaction with water.[19] However, the reaction is aggressive during exfoliation, the $LixMoS_2/LixWS_2$ compounds are extremely air sensitive, as well as the nanosheets need extensive cleaning to get rid of these impurities.[3,4,20] Most importantly, this method always induces the loss of pristine semiconducting property of MoS_2/WS_2 bulk crystals due to the structural destruction during Li intercalation.[3,17,21] Recently,

Dr. S. Xu, Dr. D. Li, Prof. P. Wu
Laboratory of Advanced Materials
State Key Laboratory of Molecular Engineering of Polymers
Department of Macromolecular Science
Fudan University
Shanghai 200433, P.R. China
E-mail: peiyiwu@fudan.edu.cn

DOI: 10.1002/adfm.201403863

Coleman et al. proposed a direct liquid exfoliation technique to synthesize few-layered MoS_2/WS_2 nanosheets with thickness of 3–12 nm by ultrasound sonication with the presence of organic solvents.[2,22] This method is green and facile, and harmless to pristine property of MoS_2/WS_2 bulk crystals. Moreover, the resulting dispersion can be directly deposited onto glassy carbon electrode (GCE) substrate for the catalysis of HER via a drop-casting method.[16]

There have been many reports focusing on the preparation of LTMDs; however, reports on synthesis of transition metal dichalcogenides quantum dots are relatively few.[8] As compared to nanosheets, quantum dots have higher special surface area and more edge atom, which is beneficial to the catalytic activity toward HER. Besides, the characteristic luminescent property of quantum dots might make transition metal dichalcogenides promising materials in biomedical and optical imaging areas.[23,24] A few works have successfully prepared MoS_2 quantum dots by high-powered ultrasonication; however, this method suffers multiple drawbacks, including long ultrasonication time, low yield, complex post-treatment process (extraction or gradient centrifugation), and lack of redispersed solvents, which impede the wide use of it.[8,25] Many works have reported that graphene or graphene oxide can be cut into graphene quantum dots by a simple hydrothermal process.[26] As MoS_2/WS_2 nanosheets are also covalently bonded 2D structure, it is not unreasonable that MoS_2/WS_2 quantum dots can also be synthesized by cutting nanosheets.[17]

Herein, uniform MoS_2/WS_2 quantum dots are prepared through solvothermal treatment of MoS_2/WS_2 nanosheets which are exfoliated by sonication with organic solvents. The as-prepared MoS_2/WS_2 quantum dots can be easily redispersed in deionized water and show strong fluorescence under UV light, which is very different from the nanosheets. These quantum dots are utilized in in vitro imaging and show good performance. Moreover, both MoS_2 and WS_2 hybrid nanostructures exhibit excellent electrocatalytic activity with low overpotential toward HER, which is mainly resulted from the enhancement of exposed active edges of MoS_2 or WS_2. Moreover, several solvents are tried to prepare MoS_2/WS_2 quantum dots, the results indicate MoS_2/WS_2 quantum dots only can be obtained in "good solvent" in which MoS_2/WS_2 nanosheet are well-dispersed. This method might present a versatile and facile pathway for industrial preparation of the quantum dots of transition metal dichalcogenides or other layered materials.

2. Results and Discussion

2.1. Preparation and Characterizations of MoS_2 and WS_2 Quantum Dots

A simple solvothermal treatment was employed to prepared MoS_2 and WS_2 quantum dots in *N,N*-dimethylformamide (DMF), as shown in **Scheme 1**. More details on the synthesis procedure can be found in the Experimental Section. The as-prepared products were settled for several hours or centrifuged for several minutes to obtain the transparent light yellow solution which exhibits strong light blue photoluminescence (PL).[25] In transmission electron microscope (TEM) images, uniform quantum dots are observed after the solvothermal treatment (**Figure 1**). The particle size distribution show the average size of MoS_2 and WS_2 quantum dots is about 3.3 and 2.5 nm, respectively (Figure 1a,b,d,e). The different size of MoS_2 and WS_2 may be resulted from the interior property of MoS_2 and WS_2 cells. The highly paralleled and ordered lattice fringe in high-resolution TEM (HRTEM) images suggest both quantum dots are well-crystallized (Figure 1c,f). The d-spacing of MoS_2 quantum dots is 0.23 nm, corresponding to the (103) faces of MoS_2 crystals, as well as the d-spacing of WS_2 quantum dots is 0.27 nm, which corresponds to the (101) faces of WS_2 crystals, indicating these quantum dots are MoS_2 or WS_2.[8,27] The aureole in selected area electron diffraction (SAED) patterns reveal these quantum dots are polycrystalline, which are different from bulk MoS_2 and WS_2, demonstrating that the destruction and exfoliation of MoS_2/WS_2 powder during solvothermal treatment. Energy dispersive X-ray spectroscopy (EDX) measurements reveal the presence of Mo, S and W, S elements in quantum dots, which further confirms that these quantum dots are MoS_2 and WS_2 (Figure S1, Supporting Information). X-ray photoelectron spectroscopy measurements were also carried out to understand the chemical state and surface composition of MoS_2 quantum dots (Figure S2, Supporting Information). The peaks at 232.6 and 229.3 eV in the high-resolution spectrum of Mo are assigned to Mo^{4+} $3d_{3/2}$ and Mo^{4+} $3d_{5/2}$, respectively, while the peaks at 163.4 and 162.3 eV in

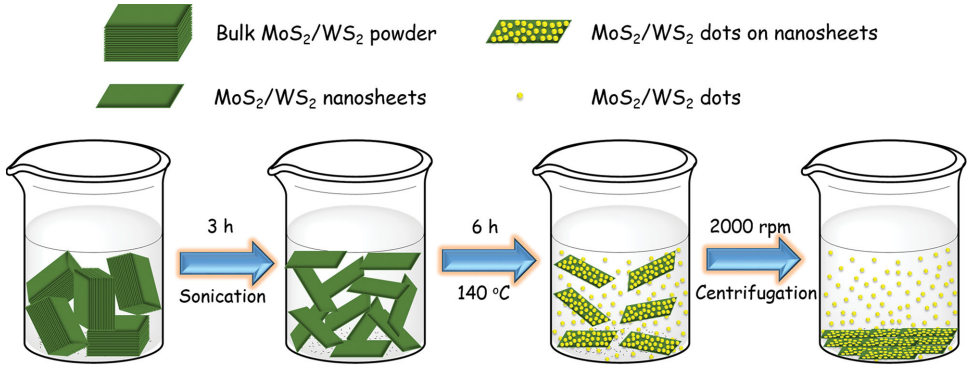

Scheme 1. Schematic representation of the synthesis process to prepare MoS_2/WS_2 quantum dots by using a liquid exfoliation and solvothermal treatment approach in DMF, NMP, and DMEU.

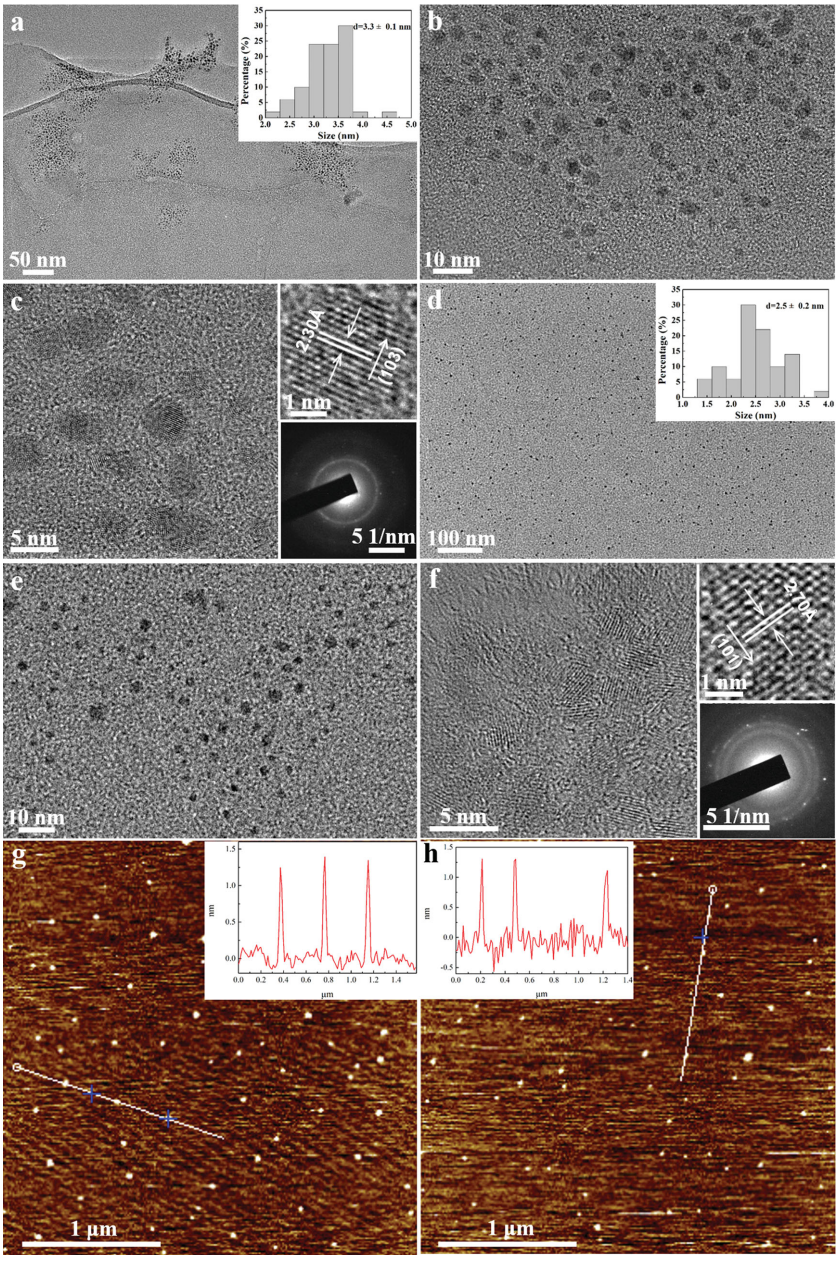

Figure 1. TEM images of a–c) MoS_2 and d–f) WS_2, and AFM images of g) MoS_2 and h) WS_2 quantum dots prepared with the sonication and solvothermal treatment of MoS_2 and WS_2 powder in DMF. Insets of (a,d): The size distribution of MoS_2 and WS_2 quantum dots. Insets of (c,f): The HRTEM images and SAED patterns of MoS_2 and WS_2 quantum dots. Insets of (g,h): the height of MoS_2 and WS_2 quantum dots.

the high-resolution spectrum of S are attributed to S $2p_{1/2}$ and S $2p_{3/2}$. A small peak locating at 235.9 eV is ascribe to Mo^{6+}, which might be originated from the slight oxidation of Mo edges during the MoS_2 exfoliation and solvothermal process.[8] Overall, the 2H phase MoS_2 quantum dots have been successfully synthesized.

To further investigate the morphology and thickness of the as-prepared quantum dots, atomic force microscopy (AFM) measurements of these nanostructures were carried out. The results show both the height of these quantum dots is about 1.2 nm, which is very close to the height of monolayer MoS_2/WS_2 (0.8–1.0 nm), suggesting that these quantum dots are monolayer (Figure 1g,h). Noticeably, the height of MoS_2 and WS_2 nanosheets which are synthesized only by the sonication of MoS_2/WS_2 powder in DMF is much bigger (3–10 nm) than quantum dots (Figure S3, Supporting Information). This result indicates the incision and further exfoliation of nanosheets during solvothermal treatment process.

Apart from DMF, another five solvents, *N*-methyl-2-pyrrolidone (NMP), dimethylimidazolidinone (DMEU), deionized water, ethanol, and acetone were also employed to investigate whether the solvents would impact the preparation of MoS_2/WS_2 quantum dots. The results show MoS_2/WS_2 quantum dots are only synthesized in "good solvent" (DMF, NMP, and DMEU) in which MoS_2/WS_2 powder can be efficiently exfoliated and well dispersed (Figure S4, Supporting Information). **Figure 2** shows the TEM images of MoS_2 and WS_2 quantum dots prepared in NMP. The quantum dots are also uniform distributed with clear and ordered lattice fringe. The average size of MoS_2 quantum dots is about 3.9 nm, slight bigger than that of WS_2 quantum dots, which is well consistent with the result in DMF (Figure 2a,c). And the d-spacing is 0.23 and 0.27 nm for MoS_2 and WS_2 quantum dots which is same as that prepared in DMF (Figure 2b,d). Furthermore, the SAED patterns also reveal these quantum dots are polycrystalline. The height of quantum dots is about 1 nm, much thinner than the nanosheets prepared with NMP, which is according to that in DMF, confirming that MoS_2/WS_2 powder can be exfoliated to monolayer quantum dots by solvothermal treatment (Figures S5 and S6, Supporting Information). As we know, both the decomposed temperature for DMF and NMP is much higher than 140 °C, thereby, these quantum dots should not be C quantum dots which are formed by the carbonization of solvents.[17] Thus, all of the results demonstrate both the quantum dots prepared in DMF and NMP are almost the same and come from MoS_2 and WS_2 crystals.

For the products prepared in DMEU, in the supernatant, not only MoS_2 quantum dots were obtained, but also some bigger particles could be found, as shown in Figure S7a, Supporting Information. The quantum dots are crystallized with the size of 3–4 nm, which is consistent with the samples in DMF and NMP (Figure S7d, Supporting Information). The morphology of bigger particles are irregular and the size of them is 40–60 nm (Figure S7b, Supporting Information).

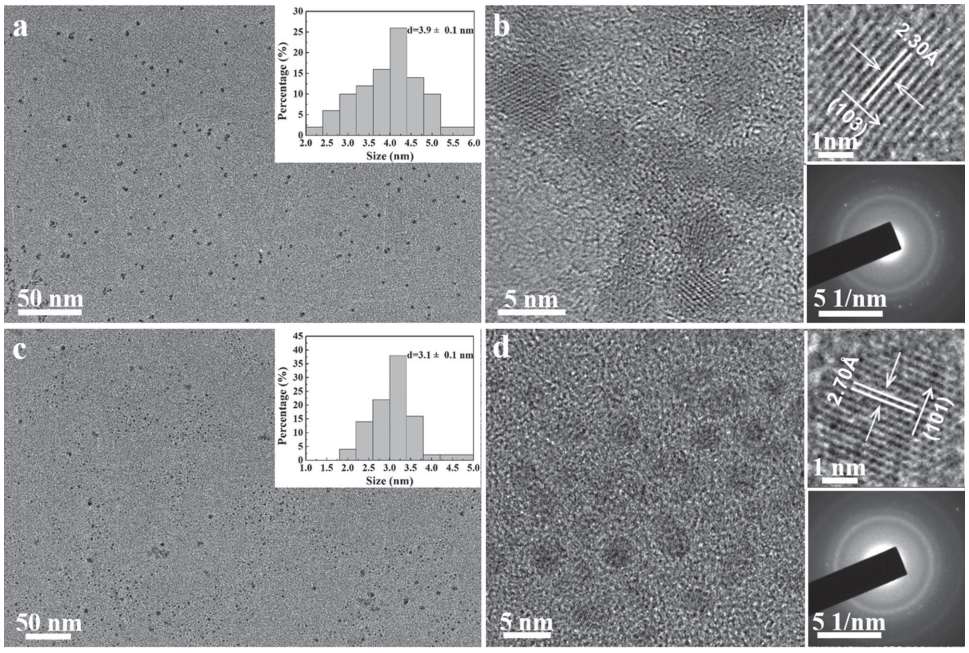

Figure 2. TEM images of a,b) MoS_2 and c,d) WS_2 quantum dots prepared with the sonication and solvothermal treatment of MoS_2 and WS_2 powder in NMP. Insets of (a,c): The size distribution of MoS_2 and WS_2 quantum dots. Insets of (b,d): The HRTEM images and SAED patterns of MoS_2 and WS_2 quantum dots.

Importantly, the magnified TEM image shows that these particles are composed of many quantum dots whose size is similar to the separated quantum dots (Figure S7c, Supporting Information). Thereby, these particles are probably the intermediates of quantum dots, that is, the MoS_2 nanosheets are first incised to bigger particles, with the increase in reaction time, the particles are further incised to quantum dots. Importantly, in some particles, we also find some amorphous region which might be resulted from the destructed edge of MoS_2 quantum dots or residual solvent between quantum dots, further confirming the incision and exfoliation of nanosheets by solvent during solvothermal treatment (Figure S8, Supporting Information). The probable reason for the appearance of bigger particles in DMEU is the dispersive capacity and cutting ability of DMEU for MoS_2 and WS_2 nanosheets is weaker than that of DMF and NMP. Since the quantum dots prepared in DMEU are not very uniform, we only focused on the further characterization and application of the uniform quantum dots prepared in DMF and NMP.

The crystal structure of these as-prepared nanosheets and quantum dots were systematically investigated by X-ray powder diffraction (XRD) patterns and Raman spectra. As shown in **Figure 3**a,b, the peak position of raw MoS_2 and WS_2 are almost the same, showing a very strong diffraction peak at $2\theta = 14.4°$ and two lower peaks at $2\theta = 39.6°$ and $2\theta = 49.8°$, which are assigned to (002), (103), and (105) faces, respectively (JCPDF (37–1492) and (84–1398)).[17,28] After ultrasonication, the signal of the (002) reflection is broadened and obviously decreased with the disappearance of most of other peaks, indicating the highly exfoliated nature of these nanosheets.[15] As we know, the peak position corresponds to the d-spacing of crystals, theoretically, if all the materials are monolayer and have no interaction between each other, there would be no signal or peak on XRD pattern. Rao et al. have already demonstrated that the characteristic peak at $2\theta = 14.4°$ disappears when MoS_2/WS_2 powder are exfoliated to monolayer nanosheets.[29] The presence of (002) reflection signal indicates most of these nanosheets are few-layer and have layer–layer interactions, which is well consistent with the results of AFM images (Figures S3 and S6, Supporting Information). After the solvothermal treatment, the few-layer nanosheets are further exfoliated and incised to monolayer quantum dots (Figures 1g,h and S4, Supporting Information). As expected, the characteristic peak at $2\theta = 14.4°$ disappears, since the quantum dots are very small and thin and hardly have layer–layer interactions between each other. A small peaks at $2\theta = 44.5°$ on the spectra of MoS_2 quantum dots, corresponding to (006) faces, are probably resulted from the partial re-stacking of quantum dots during the drying process. For WS_2 quantum dots, the disappearance of the characteristic peaks also suggests thin structure of quantum dots. And the small peak at $2\theta = 17.0°$ should come from the diffractions of impurity.[30]

Raman analysis is a universal and facile measurement to investigate the layers of MoS_2/WS_2 materials. The Raman spectrum of MoS_2 powder is well known with two main modes, the A_{1g} and the E_{2g}, located at ≈408 and ≈383 cm^{-1}, respectively (Figure 3c). The A_{1g} peak has a redshift in the order of 5 cm^{-1} from powder to monolayer. Although the peak position of E_{2g} also changes with the decrease in MoS_2 layers, the variation tendency has not yet been determined and the mechanism remains unclear at present.[2,31] As we can see, the A_{1g} peak shifts to 406.5 cm^{-1} after MoS_2 power is sonicated in DMF for 3 h, suggesting MoS_2 is exfoliated to few-layer nanosheets. While for MoS_2 sonicated in NMP, the A_{1g} peak further shifts to 405 cm^{-1} which corresponds to bilayer or trilayer structure. It means that the MoS_2 nanosheets prepared in NMP is thinner

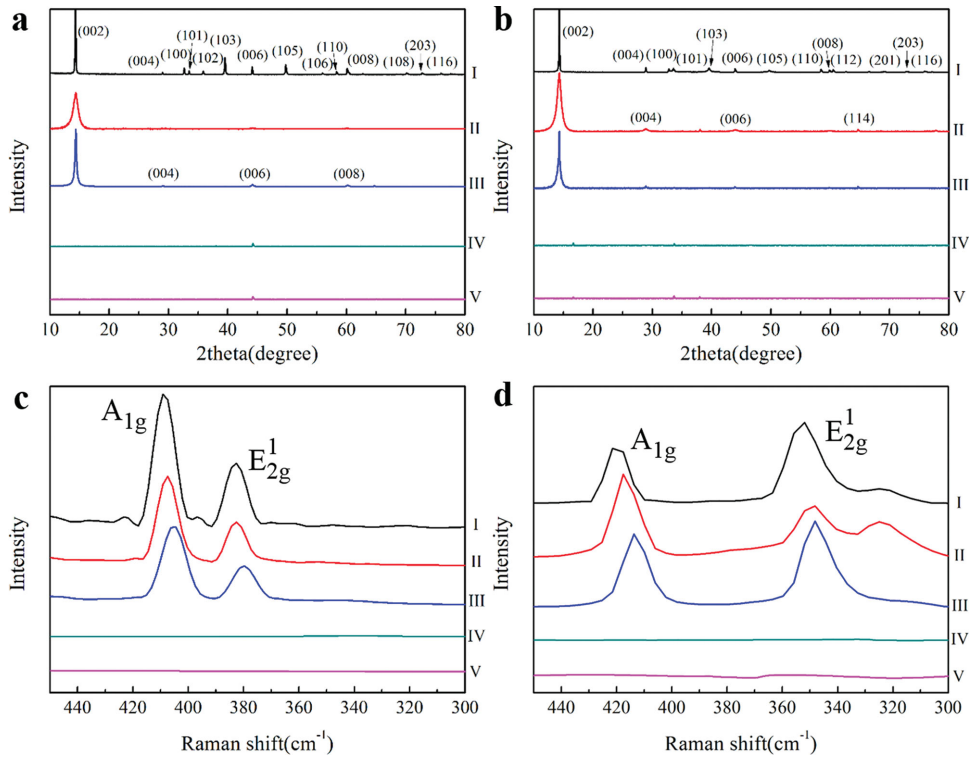

Figure 3. XRD patterns (top row) and Raman spectra (bottom row) of a,c) MoS_2 and b,d) WS_2. I) powder; II) nanosheets prepared in DMF; III) nanosheets prepared in NMP; IV) quantum dots prepared in DMF; and V) quantum dots prepared in NMP. The parameters of crystal are referenced to JCPDF (37–1492) and (84–1398).

than that prepared in DMF, that is, the exfoliation activity of NMP is better than DMF. This result is confirmed by the height of MoS_2 nanosheets in AFM images (Figures S3a and S6a, Supporting Information). On the spectra of WS_2, the bulk material also shows two intensive peaks around 420 (A_{1g}) and 353 cm^{-1} (E_{2g}) (Figure 3d).[29] The A_{1g} peak also downshifts when WS_2 powder is exfoliated to nanosheets. For the nanosheets prepared in DMF and NMP, the A_{1g} peak downshifts to 417 and 414 cm^{-1}, respectively, also revealing the exfoliation of bulk WS_2 and the better exfoliation activity of NMP (Figures S3b and S6b, Supporting Information).[32] While for the Raman spectra of MoS_2 and WS_2 quantum dots, no characteristic peak is observed, which is very different from that of powder and nanosheets. It might be caused by two factors: 1) the residual solvents which are adsorbed on quantum dots would cover the surface of quantum dots and weaken the Raman signals; 2) The absence of layer–layer interactions would sharply decrease the Raman intensity.[30,33]

2.2. Optical Properties of MoS_2 and WS_2 Quantum Dots

To further investigate the property of nanostructured MoS_2/WS_2 quantum dots, the samples were characterized by absorption spectra. **Figure 4**a shows the UV–vis spectra of MoS_2 nanosheets and quantum dots prepared in DMF and NMP. Four characteristic absorption bands are observed in the spectra of MoS_2 nanosheets. The distinct peaks at 395 and 450 nm are assigned to direct transition from the deep valence band to the conduction band, as well as the peaks at 610 and 660 nm are attributed to the K point of the Brillouin zone.[8,25,34] While on the spectra of MoS_2 quantum dots, these four characteristic peaks disappear, instead, a peak in the near-UV region (λ < 300 nm) is observed, which is assigned to the excitonic features of MoS_2 quantum dots.[35] Noticeably, the characteristic peaks of MoS_2 nanosheets and quantum dots prepared in DMF and NMP are almost the same, which demonstrates the solvent can hardly affect the chemical state of MoS_2 nanosheets or quantum dots. This result is confirmed by the UV–vis spectra of WS_2 nanosheets and quantum dots (Figure S9a, Supporting Information). The PL spectra of MoS_2 quantum dots show a strong emission maximum at 463 nm under the excitation wavelength of 390 nm (Figure 4b). For WS_2 quantum dots, the maximum excitation and emission wavelength slightly shifts to 410 and 485 nm (Figure S9b, Supporting Information). As the excitation wavelength ranges from 320 to 460 nm, the PL peak of MoS_2 quantum dots shifts to longer wavelength from 440 to 520 nm (Figure 4c,d). The variation of peak position and intensity of MoS_2/WS_2 quantum dots prepared in DMF and NMP are almost the same, further demonstrating that the solvent has little or no effect on the chemical property of these quantum dots (Figures S9c and S9d, Supporting Information). To investigate the photo stability of MoS_2 and WS_2 quantum dots, the photoluminescenece intensity of them is measured after UV irradiation (365 nm) for different time. The photoluminescenece intensity of MoS_2 and WS_2 quantum dots is almost unchanged after UV irradiation for 24 h and still >78% after 72 h UV irradiation. While for the commercial fluorochrome–fluorescein

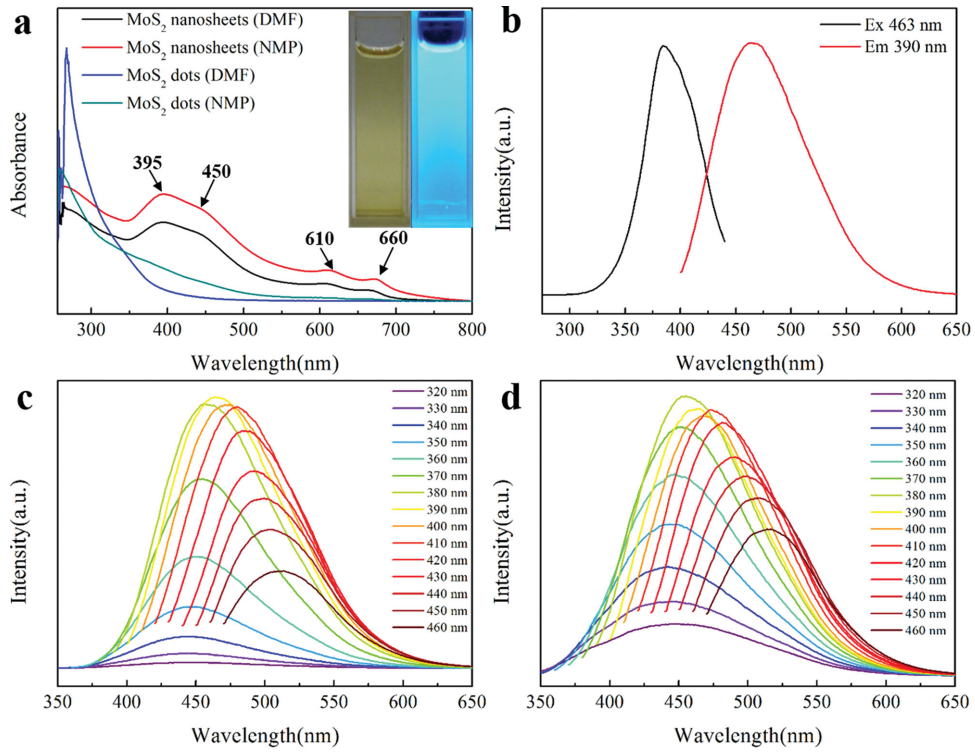

Figure 4. a) UV–vis spectra of MoS_2 nanosheets and quantum dots prepared in DMF and NMP; b) excitation and emission PL spectra of MoS_2 quantum dots; c) emission PL spectra of MoS_2 quantum dots prepared in DMF; and d) emission PL spectra of MoS_2 quantum dots prepared in NMP.

isothiocyanate, the normalized intensity is sharply decreased to 18% after 72 h UV irradiation (Figure S10, Supporting Information). This result reveals that the as-prepared MoS_2 and WS_2 quantum dots have excellent photo stability.

2.3. Bioimaging with MoS_2 and WS_2 Quantum Dots

Due to the dried MoS_2/WS_2 quantum dots can easily redispersed in water and exhibit strong fluorescence. The possible application of these water-soluble quantum dots as cell-imaging agents was explored. The inherent cytotoxicity of MoS_2/WS_2 quantum dots were evaluated using two living cell lines (HEK 293T cell lines and HeLa cell lines) through MTT (MTT = 3-(4,5-dimethylthiazol-2-yl)-2,5-diphenyltetrazolium bromide) assay. The cell viabilities of two cells were measured after they were mixed with MoS_2/WS_2 quantum dots at different concentration for 24 h. As expected, the cell viabilities of HeLa cells and HEK 293T cells decline only by <6% and <1%, respectively, when the addition of WS_2 quantum dots probes at 250 μg mL^{-1}, which is comparable to or even better than many fluorescent carbon nanoparticles.[24,36] Besides, in HeLa cells and HEK 293T cells, the cell viabilities are both >77% upon addition of the fluorescent probes at up to 2000 μg mL^{-1}, indicating the greatly low cytotoxicity of WS_2 quantum dots (Figure S11, Supporting Information). For MoS_2 quantum dots, the reduction in cell viability of HeLa is about 1% and 12% meanwhile the reduction in cell viability of HeLa cells is about 11% and 30%, when the probes concentration is 250 and 2000 μg mL^{-1}, also revealing these quantum dots are harmless to cells. Comparing with the MoS_2 nanosheets reported by Xu et al.,[37] whose cell viability is lower than 83% just in 250 μg mL^{-1}, our MoS_2/WS_2 quantum dots show much bettter biocompatibility.

To determine the cell permeability of the probes, HeLa cells were incubated in Dulbecco's modified Eagle's medium (DMEM) containing 50 μg mL^{-1} of MoS_2/WS_2 quantum dots for 7 h at 37 °C, and the extracellular remaining quantum dots were removed by washing with phosphate buffer solution (PBS). The MoS_2/WS_2 quantum dots incubated HeLa cells show a remarkable intracellular fluorescence in the confocal laser scanning microscopy (CLSM) image (**Figure 5**). Obviously, the fluorescence of MoS_2/WS_2 probes and LysoTracker in cells can overlap very well, which indicates that MoS_2/WS_2 quantum dots should enter into cells by endocytosis. Moreover, the fluorescent spots are observed only in the cell membrane and the perinuclear regions of the cytosol, but are very weak at the central region corresponding to the nucleus, suggesting that the MoS_2/WS_2 quantum dots can easily permeate into the cell but cannot penetrate into the nuclei. Thus, the genetic sequence disruption does not occur, further confirming the low cytotoxicity of these probes. Based on above results, undoubtedly, these as-prepared MoS_2/WS_2 quantum dots can be considered to be promising, low toxic, biocompatible, and good cell-permeability probes for in vitro imaging.

2.4. Electrocatalysis Application of MoS_2 and WS_2 Composites

Previous work has demonstrated that MoS_2 quantum dots are favorite to intersperse in nanosheets.[8] Comparing with

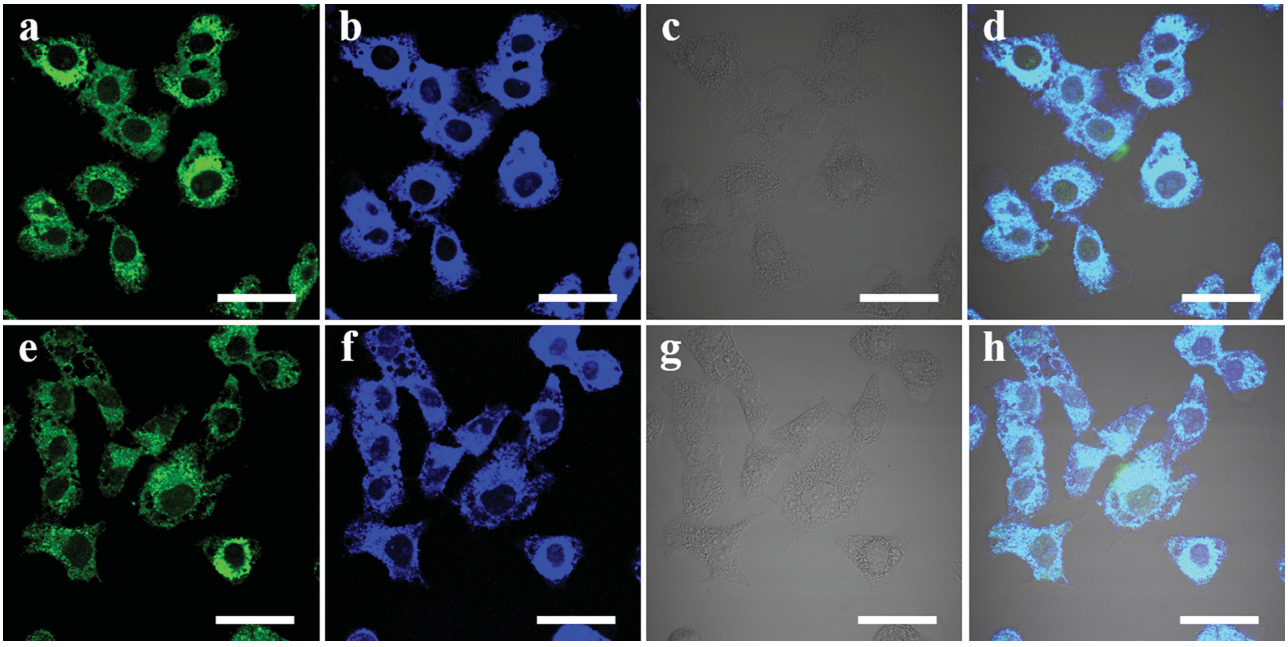

Figure 5. a,e) Confocal laser scanning microscopy image of HeLa living cells stained with 0.001 mg mL^{-1} of LysoTracker for 20 min; b,f) Confocal laser scanning microscopy image of HeLa living cells incubated in DMEM containing 50 μg mL^{-1} b) MoS_2 and f) WS_2 for 7 h at 37 °C. c,g) The corresponding brightfield image and d,h) overlapped image of the living cells. All scale bars are 40 μm.

Shaijumon's work, the preparation method of MoS_2 quantum dots interspersed MoS_2 nanosheets in our work is more convenient and does not need special equipment. MoS_2 quantum dots and MoS_2 quantum dots interspersed MoS_2 nanosheets can be prepared simultaneously only by ordinary sonication and solvothermal process. In TEM images, the MoS_2 and WS_2 nanosheets can be obviously observed (Figure S12a,d, Supporting Information). The size of them is 1–2 μm, which is well consistent with the MoS_2 nanosheets prepared by liquid exfoliation in other works.[2,16,22] The magnified TEM images show plenty of quantum dots are interspersed in nanosheets (Figure S12b,e, Supporting Information). The ordered lattice fringe in HRTEM images and aureole in SAED patterns reveal these quantum dots are polycrystalline. The d-spacings of them are 0.23 and 0.27 nm which is same as the data in Figure 1, demonstrating these quantum dots are MoS_2 and WS_2 quantum dots (Figure S12c,f, Supporting Information). Moreover, the EDX patterns and element mapping images further confirm these composites are MoS_2 and WS_2 composites (Figure S13, Supporting Information). These results mean that the composites of MoS_2/WS_2 nanosheets and quantum dots also can be obtained as byproducts during the preparation of MoS_2/WS_2 quantum dots.

As a typical application, MoS_2 and WS_2 materials were explored as electrocatalysts for HER. The HER activity of these materials was measured using the standard three electrode electrochemical configuration in 0.5 M sulfuric acid (H_2SO_4) electrolyte with a scan rate of 5 mV s^{-1}, as described in previous reports.[10,15,16] As shown in **Figure 6**a, the MoS_2 and WS_2 suspension obtained after 3 h sonication exhibit overpotential value of >350 mV which is slightly higher than the value reported in other works.[12,38] The probable reason is that we directly drop the suspension of MoS_2/WS_2 onto GCE after 3 h sonication. As we know, MoS_2 is a poor HER catalyst in its bulk form, thereby, many bulk MoS_2/WS_2 or nanosheets with dozens of layers which might be residual on electrode should decrease the catalyst activity of nanosheets with monolayer or few-layer.[27] After the solvothermal process, the MoS_2 composites (composite of nanosheets and quantum dots) show a smaller onset overpotential of ≈120 mV for HER, beyond which the cathodic current enhances rapidly under more negative potential. This onset overpotential is close to or even smaller than that of the monolayer or few-layer MoS_2 nanosheets with many active sites.[10,16,39] The excellent catalytic activity of these MoS_2 composites may arise from two factors: (1) the MoS_2 quantum dots interspersed in MoS_2 nanosheets possess unique defect-rich structure which brings in more active edge sites for HER; (2) the random or disordered stacking of the exfoliated MoS_2 nanosheets on the surface of glass carbon electrode may enhance the efficiency of electron transfer between the active edge sites and underlying electrode.[12,16] The onset overpotential of WS_2 composites is ≈180 mV for HER, which is slightly poorer than MoS_2 composites. In fact, plenty of works have already demonstrated that WS_2 is inferior to MoS_2 in electrocatalytic activity toward HER if they have same or similar nanostructures.[40] However, the catalytic activity of WS_2 composites in our work is comparable to or even better than many other WS_2 materials, such as WS_2 nanosheets, nanoribbons, nanotubes, etc.[15,27,32,40,41] The remarkable catalytic activity of MoS_2 and WS_2 composites suggests that the combination of sonication and solvothermal treatment might be a versatile method to prepared excellent transition metal dichalcogenides based catalysts toward HER.

Interestingly, the onset overpotential of MoS_2/WS_2 composites prepared in DMF and NMP are same, which strongly confirms the solvent has little or no effect on the chemical property

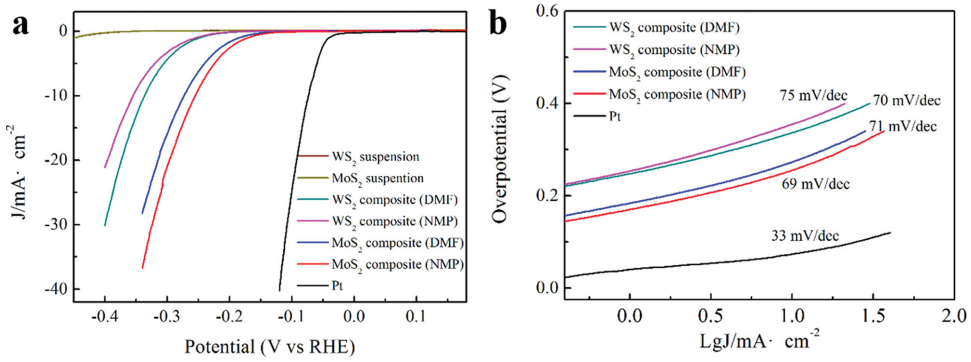

Figure 6. HER activity of exfoliated MoS_2/WS_2 materials. a) Polarization curves of MoS_2/WS_2 suspension (after 3 h sonication) and composites (composites of nanosheets and quantum dots); b) Corresponding Tafel plots obtained from the polarization curves. Tafel slopes of ≈33 and 69–75 mV dec^{-1} have been measured for commercial Pt and MoS_2/WS_2 composites, respectively.

and structure of these quantum dots. The slightly higher current density of the samples prepared in NMP might be resulted from the more quantum dots are formed and interspersed in nanosheets in NMP. We have measured the maximum concentration of MoS_2 and WS_2 in DMF and NMP after exfoliation and centrifugation by weight method, the results show the concentration of MoS_2/WS_2 in NMP is much higher than that in DMF, suggesting that the exfoliation and activity of NMP is better (Table S1, Supporting Information). It is not unreasonable that more quantum dots are incised and interspersed in nanosheets in NMP.

Tafel slope is an intrinsic property of the electrocatalyst materials that is determined by the rate-limiting step of the HER. The Tafel slopes are determined by Tafel plots where their linear portions are fit to the Tafel equation ($\eta = b \times \log j + a$, in which j is the current density and b is the Tafel slope). Figure 6b shows the Tafel plots for the MoS_2/WS_2 composites and commercial Pt. The Tafel slope of commercial Pt (20 wt% Pt/C) is ≈33 mV dec^{-1}, which is close to the previous work.[12,40] For MoS_2 and WS_2 composites, the Tafel slopes range from 69 to 75 mV dec^{-1} which are comparable to that reported in 1T phase WS_2 nanosheets and slightly poorer than 1T phase MoS_2 nanosheets.[10,15,41] Comparing with the commercially available MoS_2 (115 mV dec^{-1}) and WS_2 (138 mV dec^{-1}) catalysts, the Tafel slopes of MoS_2 and WS_2 composites are much smaller in our work.[42] For practical applications, the small Tafel slope is advantageous, as it results in the faster enhancement of HER rate with the increase in overpotential.[43] On the other hand, the life-time or durability of electrocatalysts is also a very important factor to evaluate the catalytic activity. Figure S14, Supporting Information shows the comparison polarization curves for the MoS_2 catalysts in the initial and after 2000 cycles. The almost identical curves suggest the excellent durability and good catalytic stability for these composites. Thereby, these materials can substitute commercial Pt as promising electrocatalysts toward HER.

3. Conclusion

In summary, we reported a facile and green technique to prepare uniform and monolayer MoS_2 and WS_2 quantum dots by the combination of sonication and solvothermal treatment of bulk MoS_2 and WS_2 at a mild temperature. The results showed that MoS_2/WS_2 quantum dots were only synthesized in "good solvent" in which MoS_2/WS_2 powder can be efficiently exfoliated and well dispersed, the solvent had little or no effect on the chemical property of these quantum dots, and NMP had better exfoliation and incision activity than DMF and DMEU for MoS_2/WS_2 powder. These quantum dots showed strong fluorescence, good cell permeability, and low cytotoxicity in living cells, which made them promising materials for in vitro bioimaging. The larger concentration of active sites resulting from the unique monolayer and defect-rich nanostructures of MoS_2/WS_2 quantum dots rendered good HER catalytic activity of these composites, showing a small onset overpotential, along with long-term durability. Therefore, it could be a promising and alternative non-Pt catalyst to replace Pt-based catalysts toward HER. Furthermore, this technique might provide a versatile approach to synthesize the quantum dots of transition metal dichalcogenides or other layered materials on a large scale.

4. Experimental Section

Materials: MoS_2 and WS_2 were purchased from Aladdin industrial corporation. DMF, NMP, DMEU, ethanol, acetone, and H_2SO_4 (98%) were supplied from Sinopharm Chemical Reagent Co. Ltd. Nafion solution (5%) was purchased from Sigma–Aldrich. All reagents were of analytical grade and used without further purification. N_2 with a purity of 99.9% was purchased from Shanghai Jifu Gas Co. Ltd.

Preparation of MoS_2/WS_2 Quantum Dots: Bulk MoS_2/WS_2 powder was first exfoliated to nanosheets by solvent exfoliation method.[2] Typically, 1 g of MoS_2/WS_2 powder and 100 mL of DMF were added in 150 mL serum bottle and kept sonication for 3 h to exfoliate MoS_2/WS_2 powder by sonicator (KQ5200DB) with an output power of 250 W. Then the top 2/3 of the dispersion was decanted into flask and kept vigorous stirring for 6 h at 140 °C. Afterwards, the resulting suspensions were settled for several hours or centrifuged for 5 min at 2000 rpm to separate the centrifugate and supernatant. The light yellow supernatant was MoS_2/WS_2 quantum dots and the centrifugate was the composite of MoS_2/WS_2 quantum dots and nanosheets. The yields of MoS_2 and WS_2 quantum dots from nanosheets suspension is about 13 and 18 wt%, respectively. Both centrifugate and supernatant were collected for further characterization. Part of supernatant was evaporated under

vacuum at a certain temperature to remove the excessive solvent and redispersed in water for further use. Six solvents were employed to investigate whether the solvents would impact the preparation of MoS_2/WS_2 quantum dots. DMF, NMP, and DMEU were the "good solvent" in which MoS_2/WS_2 nanosheets were well dispersed, as well as deionized water, ethanol, and acetone were the "poor solvent." The results show MoS_2/WS_2 powder only can be exfoliated to nanosheets and further incised to quantum dots in "good solvent." In "poor solvent," they are still powder after sonication and heating.

Cell Culture and MTT Assay: The cellular cytotoxicity of MoS_2/WS_2 quantum dots was tested on HEK 293T and HeLa cells, which was referred to our previous work.[44] Typically, HeLa cells were routinely cultured in flasks and incubated at 37 °C in a humidified hood filled with 5% CO_2. Each flask contained 10 mL of DMEM (High Glucose) supplemented with 10% fetal bovine serum, penicillin (100 U mL^{-1}), and streptomycin (100 U mL^{-1}). When cells reached 80%–90% confluence, they were lifted with trypsin-EDTA. The trypsinized cells were dispersed and diluted in DMEM (High Glucose) medium, followed by centrifugation for 5 min at 1000 rpm. After supernatant was removed, the cells were resuspended in DMEM (High Glucose) medium and cells number was counted using a hemocytometer. Cells were then plated at a density of approximately 2×10^4 cells per well in a 96-well plate. A 100 µL of medium was added to each well. Cells were subsequently incubated at 37 °C in a 5% CO_2 humid incubator for 24 h. The number of viable cells was determined by MTT assay with 3-(4,5-dimethylthiazole-2-yl)-2,5-phenyltetrazolium bromide. MoS_2/WS_2 quantum dots were added to the wells in increasing concentrations at 250, 500, 1000, and 2000 µg mL^{-1}, respectively. Cells were incubated for 24 h at 37 °C. Then, 20 µL (5 mg mL^{-1}) of MTT solution was added to each well and the plate was further incubated for 4 h to deoxidize MTT. After incubation, the medium was aspirated out and 150 µL of DMSO was added into each well. Absorbance was measured at 570 nm in a Multiskan MK3 microplate photometer (Thermo Scientific, USA). The cells cultured with the pure culture medium were set as controls. Measure the absorbance on an ELISA plate reader with a test wavelength of 570 nm and a reference wavelength of 630 nm to obtain sample signal (OD_{570}-OD_{630}).

In Vitro Cell Experiments: HeLa cells were incubated in ϕ – 15 mm thin bottom culture chambers with 50 µg mL^{-1} of MoS_2 or WS_2 quantum dots. After 7 h incubation, the cell were washed with DMEM and PBS (pH = 7.4) for three times to remove the extracellular remaining MoS_2/WS_2 quantum dots, followed by 0.001 mg mL^{-1} of LysoTracker stained for 20 min. After LysoTracker was removed by PBS washing, the sample was observed by CLSM with excitation wavelengths of 405 and 488 nm.

Electrochemical Measurements: Electrochemical measurements were carried out with a computer-controlled potentiostat (CHI660D) in a standard three-electrode cell using saturated calomel electrode as the reference electrode, a platinum wire as the counter electrode and a GCE as the working electrode. The working electrode was prepared as reported in our previous work.[45] In brief, 5 µL of 0.5 mg mL^{-1} MoS_2 suspension (composite of nanosheets and quantum dots) was dropped onto a GCE with 3 mm diameter and 5 µL of Nafion solution (5 wt%) was coated after the suspensions was dried. Linear sweep voltamperometry was performed in 0.5 M H_2SO_4 solution deaerated with N_2 with a scan rate of 5 mV s^{-1}.

Characterization: The TEM images were taken with a JEOL JEM2011 at 200 kV equipped with SAED. AFM images were obtained by using a Multimode Nano4 in the tapping mode after the samples were deposited on a freshly cleaved mica surface by spin coating. Field emission scanning electron microscope observations were performed on Zeiss Ultra 55 with gold coating with EDX. XRD data were acquired by a D8 ADVANCE and DAVINCI.DESIGN (Bruker) X'pert diffractometer with Cu K_α radiation. Fluorescence spectroscopy was carried out with a Shimadzu RF-5301PC spectrophotometer. Raman spectra were recorded on XploRA Laser Raman spectrometer equipped with 638 nm helium/neon laser and CCD (charge-coupled device) detector. The UV–vis spectra were recorded on a Hitachi U-2910 spectrophotometer.

Supporting Information

Supporting Information is available from the Wiley Online Library or from the author.

Acknowledgements

The authors gratefully acknowledge the financial support of the National Science Foundation of China (NSFC) (20934002 and 20774022) and the National Basic Research Program of China (No. 2009CB930000). The authors also thank the great help from the group of Professor Changchun Wang.

Received: November 2, 2014
Revised: November 26, 2014
Published online: January 8, 2015

[1] a) Y. Sun, Q. Wu, G. Shi, *Energ. Environ. Sci.* **2011**, *4*, 1113; b) C. Lee, Q. Li, W. Kalb, X.-Z. Liu, H. Berger, R. W. Carpick, J. Hone, *Science* **2010**, *328*, 76; c) M. Osada, T. Sasaki, *Adv. Mater.* **2012**, *24*, 210.

[2] J. N. Coleman, M. Lotya, A. O'Neill, S. D. Bergin, P. J. King, U. Khan, K. Young, A. Gaucher, S. De, R. J. Smith, I. V. Shvets, S. K. Arora, G. Stanton, H.-Y. Kim, K. Lee, G. T. Kim, G. S. Duesberg, T. Hallam, J. J. Boland, J. J. Wang, J. F. Donegan, J. C. Grunlan, G. Moriarty, A. Shmeliov, R. J. Nicholls, J. M. Perkins, E. M. Grieveson, K. Theuwissen, D. W. McComb, P. D. Nellist, V. Nicolosi, *Science* **2011**, *331*, 568.

[3] G. Eda, H. Yamaguchi, D. Voiry, T. Fujita, M. Chen, M. Chhowalla, *Nano Lett.* **2011**, *11*, 5111.

[4] G. S. Bang, K. W. Nam, J. Y. Kim, J. Shin, J. W. Choi, S.-Y. Choi, *ACS Appl. Mater. Interfaces* **2014**, *6*, 7084.

[5] L. Sun, Y. Ying, H. Huang, Z. Song, Y. Mao, Z. Xu, X. Peng, *ACS Nano* **2014**, *8*, 6304.

[6] Y. Shi, W. Zhou, A.-Y. Lu, W. Fang, Y.-H. Lee, A. L. Hsu, S. M. Kim, K. K. Kim, H. Y. Yang, L.-J. Li, J.-C. Idrobo, J. Kong, *Nano Lett.* **2012**, *12*, 2784.

[7] K. F. Mak, C. Lee, J. Hone, J. Shan, T. F. Heinz, *Phys. Rev. Lett.* **2010**, *105*, 136805.

[8] D. Gopalakrishnan, D. Damien, M. M. Shaijumon, *Acs Nano* **2014**, *8*, 5297.

[9] a) T. Liu, C. Wang, X. Gu, H. Gong, L. Cheng, X. Shi, L. Feng, B. Sun, Z. Liu, *Adv. Mater.* **2014**, *26*, 3433; b) L. Cheng, J. Liu, X. Gu, H. Gong, X. Shi, T. Liu, C. Wang, X. Wang, G. Liu, H. Xing, W. Bu, B. Sun, Z. Liu, *Adv. Mater.* **2014**, *26*, 1886.

[10] D. Voiry, M. Salehi, R. Silva, T. Fujita, M. Chen, T. Asefa, V. B. Shenoy, G. Eda, M. Chhowalla, *Nano Lett.* **2013**, *13*, 6222.

[11] X. Sun, J. Dai, Y. Guo, C. Wu, F. Hu, J. Zhao, X. Zeng, Y. Xie, *Nanoscale* **2014**, *6*, 8359.

[12] J. Xie, H. Zhang, S. Li, R. Wang, X. Sun, M. Zhou, J. Zhou, X. W. Lou, Y. Xie, *Adv. Mater.* **2013**, *25*, 5807.

[13] a) X. Huang, Z. Zeng, S. Bao, M. Wang, X. Qi, Z. Fan, H. Zhang, *Nat. Commun.* **2013**, *4*, 1444; b) J. Yang, D. Voiry, S. J. Ahn, D. Kang, A. Y. Kim, M. Chhowalla, H. S. Shin, *Angew. Chem. Int. Ed.* **2013**, *52*, 13751.

[14] X. Huang, Z. Zeng, H. Zhang, *Chem. Soc. Rev.* **2013**, *42*, 1934.

[15] D. Voiry, H. Yamaguchi, J. Li, R. Silva, D. C. B. Alves, T. Fujita, M. Chen, T. Asefa, V. B. Shenoy, G. Eda, M. Chhowalla, *Nat. Mater.* **2013**, *12*, 850.

[16] S. Ji, Z. Yang, C. Zhang, Z. Liu, W. W. Tjiu, I. Y. Phang, Z. Zhang, J. Pan, T. Liu, *Electrochim. Acta* **2013**, *109*, 269.

[17] V. Stengl, J. Henych, *Nanoscale* **2013**, *5*, 3387.

[18] a) Z. Yin, H. Li, H. Li, L. Jiang, Y. Shi, Y. Sun, G. Lu, Q. Zhang, X. Chen, H. Zhang, *ACS Nano* **2011**, *6*, 74; b) Y.-H. Lee, X.-Q. Zhang, W. Zhang, M.-T. Chang, C.-T. Lin, K.-D. Chang, Y.-C. Yu, J. T. -W. Wang, C.-S. Chang, L.-J. Li, T.-W. Lin, *Adv. Mater.* **2012**, *24*, 2320.
[19] Q. Wang, D. O'Hare, *Chem. Rev.* **2012**, *112*, 4124.
[20] A. A. Jeffery, C. Nethravathi, M. Rajamathi, *J. Phys. Chem. C* **2014**, *118*, 1386.
[21] J. Heising, M. G. Kanatzidis, *J. Am. Chem. Soc.* **1999**, *121*, 638.
[22] A. O'Neill, U. Khan, J. N. Coleman, *Chem. Mater.* **2012**, *24*, 2414.
[23] Z.-C. Yang, M. Wang, A. M. Yong, S. Y. Wong, X.-H. Zhang, H. Tan, A. Y. Chang, X. Li, J. Wang, *Chem. Commun.* **2011**, *47*, 11615.
[24] Y. Yang, J. Cui, M. Zheng, C. Hu, S. Tan, Y. Xiao, Q. Yang, Y. Liu, *Chem. Commun.* **2012**, *48*, 380.
[25] T. Wang, L. Liu, Z. Zhu, P. Papakonstantinou, J. Hu, H. Liu, M. Li, *Energ. Environ. Sci.* **2013**, *6*, 625.
[26] a) D. Pan, J. Zhang, Z. Li, M. Wu, *Adv. Mater.* **2010**, *22*, 734; b) Q. Wang, H. Zheng, Y. Long, L. Zhang, M. Gao, W. Bai, *Carbon* **2011**, *49*, 3134; c) Y. Sun, S. Wang, C. Li, P. Luo, L. Tao, Y. Wei, G. Shi, *Phys. Chem. Chem. Phys.* **2013**, *15*, 9907.
[27] J. Lin, Z. Peng, G. Wang, D. Zakhidov, E. Larios, M. J. Yacaman, J. M. Tour, *Adv. Energy Mater.* **2014**, *4*, 1301875.
[28] B. L. Li, L. X. Chen, H. L. Zou, J. L. Lei, H. Q. Luo, N. B. Li, *Nanoscale* **2014**, *6*, 9831.
[29] H. S. S. R. Matte, A. Gomathi, A. K. Manna, D. J. Late, R. Datta, S. K. Pati, C. N. R. Rao, *Angew. Chem. Int. Ed.* **2010**, *49*, 4059.
[30] L. Lin, Y. Xu, S. Zhang, I. M. Ross, A. C. M. Ong, D. A. Allwood, *ACS Nano* **2013**, *7*, 8214.
[31] S. Najmaei, Z. Liu, P. M. Ajayan, J. Lou, *Appl. Phys. Lett.* **2012**, *100*, 013106.
[32] L. Cheng, W. Huang, Q. Gong, C. Liu, Z. Liu, Y. Li, H. Dai, *Angew. Chem. Int. Ed.* **2014**, *53*, 7860.
[33] a) A. Molina-Sánchez, L. Wirtz, *Phys. Rev. B* **2011**, *84*, 155413; b) H. R. Gutierrez, N. Perea-Lopez, A. L. Elias, A. Berkdemir, B. Wang, R. Lv, F. Lopez-Urias, V. H. Crespi, H. Terrones, M. Terrones, *Nano Lett.* **2013**, *13*, 3447.
[34] J. P. Wilcoxon, P. P. Newcomer, G. A. Samara, *J. Appl. Phys.* **1997**, *81*, 7934.
[35] a) J. P. Wilcoxon, G. A. Samara, *Phys. Rev. B* **1995**, *51*, 7299; b) V. Chikan, D. F. Kelley, *J. Phys. Chem. B* **2002**, *106*, 3794.
[36] a) P.-C. Hsu, H.-T. Chang, *Chem. Commun.* **2012**, *48*, 3984; b) W. Li, Z. Zhang, B. Kong, S. Feng, J. Wang, L. Wang, J. Yang, F. Zhang, P. Wu, D. Zhao, *Angew. Chem. Int. Ed.* **2013**, *52*, 8151.
[37] N. Wang, F. Wei, Y. Qi, H. Li, X. Lu, G. Zhao, Q. Xu, *ACS Appl. Mater. Interfaces* **2014**, *6*, 19888.
[38] Z. Wu, B. Fang, Z. Wang, C. Wang, Z. Liu, F. Liu, W. Wang, A. Alfantazi, D. Wang, D. P. Wilkinson, *ACS Catal.* **2013**, *3*, 2101.
[39] Y. Yan, B. Xia, X. Ge, Z. Liu, J.-Y. Wang, X. Wang, *ACS Appl. Mater. Interfaces* **2013**, *5*, 12794.
[40] Z. Wu, B. Fang, A. Bonakdarpour, A. Sun, D. P. Wilkinson, D. Wang, *Appl. Catal. B* **2012**, *125*, 59.
[41] M. A. Lukowski, A. S. Daniel, C. R. English, F. Meng, A. Forticaux, R. J. Hamers, S. Jin, *Energ. Environ. Sci.* **2014**, *7*, 2608.
[42] J. Bonde, P. G. Moses, T. F. Jaramillo, J. K. Norskov, I. Chorkendorff, *Faraday Discuss.* **2008**, *140*, 219.
[43] D. Merki, X. Hu, *Energ. Environ. Sci.* **2011**, *4*, 3878.
[44] Z. Zhang, S. Xu, P. Wu, *Part. Part. Syst. Charact.* **2014**, DOI: 10.1002/ppsc.201400136.
[45] S. Xu, L. Yong, P. Wu, *ACS Appl. Mater. Interfaces* **2013**, *5*, 654.